

A peer-reviewed version of this preprint was published in PeerJ on 15 November 2019.

[View the peer-reviewed version](https://peerj.com/articles/matsci-2) (peerj.com/articles/matsci-2), which is the preferred citable publication unless you specifically need to cite this preprint.

Ferreira HM, Lopes EB, Malta JF, Ferreira LM, Casimiro MH, Santos L, Pereira MFC, Pereira Gonçalves A. 2019. Preparation, thermal stability and electrical transport properties of vaesite, NiS₂. PeerJ Materials Science 1:e2 <https://doi.org/10.7717/peerj-matsci.2>

Preparation, thermal stability and electrical transport properties of vaesite, NiS₂

Helena M Ferreira¹, Elsa B Lopes¹, José F Malta^{1,2}, Luís M Ferreira¹, Maria H Casimiro¹, Luís Santos³, Manuel FC Pereira⁴, Antonio Pereira Gonçalves^{Corresp. 1}

¹ C2TN, Departamento de Engenharia e Ciências Nucleares, Instituto Superior Técnico, Universidade de Lisboa, Bobadela, Portugal

² CFisUC, Departamento de Física, Universidade de Coimbra, Coimbra, Portugal

³ CQE, Departamento de Engenharia Química, Instituto Superior Técnico, Universidade de Lisboa, Lisboa, Portugal

⁴ CERENA, Departamento de Engenharia Civil Arquitectura e Georrecursos, Instituto Superior Técnico, Universidade de Lisboa, Lisboa, Portugal

Corresponding Author: Antonio Pereira Gonçalves
Email address: apg@ctn.tecnico.ulisboa.pt

Vaesite, a nickel chalcogenide with NiS₂ formula, has been synthesized and studied by theoretical and experimental methods. NiS₂ was prepared by solid-state reaction under vacuum and densified by hot-pressing, at different consolidation conditions. Dense single-phase pellets (relative densities >94%) were obtained, without significant lattice distortions for different hot-pressing conditions. The thermal stability of NiS₂ was studied by thermogravimetric analysis. Both as-synthesized and hot-pressed NiS₂ have a single phase nature, although some hot-pressed samples had traces of the sulfur deficient phase, Ni_{1-x}S (<1%vol), due to the strong desulfurization at T > 340°C. The electronic band structure and density of states were calculated by Density Functional Theory (DFT), indicating a metallic behavior. However, the electronic transport measurements showed p-type semiconductivity for bulk NiS₂, verifying its characteristic behavior has a Mott insulator. The consolidation conditions strongly influence the electronic properties, with the best room-temperature Seebeck coefficient, electrical resistivity and power factor being 182µVK⁻¹, 2257µΩm and 14.1µWK⁻²m⁻¹, respectively, pointing this compound as a good starting point for a new family of thermoelectric materials.

1 **Preparation, thermal stability and electrical transport**
2 **properties of vaesite, NiS₂**

3
4

5 Helena Maçarico Ferreira¹, Elsa Branco Lopes¹, José F. Malta^{1,2}, Luís M. Ferreira¹, Maria
6 Helena Casimiro¹, Luís Santos³, Manuel F.C. Pereira⁴, António Pereira Gonçalves¹

7

8 ¹ C²TN, Department of Nuclear Sciences and Engineering, Instituto Superior Técnico, University
9 of Lisbon, Portugal

10 ² CFisUC, Department of Physics, University of Coimbra, Portugal

11 ³ Centro de Química Estrutural, Instituto Superior Técnico, University of Lisbon, Lisbon,
12 Portugal

13 ⁴ CERENA – Centro de Recursos Naturais e Ambiente, Instituto Superior Técnico, University of
14 Lisbon, Lisbon, Portugal

15

16

17 Corresponding Author:

18 António Pereira Gonçalves¹

19 Estrada Nacional 10, 2695-066 Bobadela, Portugal

20 Email address: apg@ctn.tecnico.ulisboa.pt

21

22

23

24

25

26

27

28

29

30

31

32

33

34

35

36

37

38

39 Abstract

40 Vaesite, a nickel chalcogenide with NiS₂ formula, has been synthesized and studied by
41 theoretical and experimental methods. NiS₂ was prepared by solid-state reaction under vacuum
42 and densified by hot-pressing, at different consolidation conditions. Dense single-phase pellets
43 (relative densities >94%) were obtained, without significant lattice distortions for different hot-
44 pressing conditions. The thermal stability of NiS₂ was studied by thermogravimetric analysis.
45 Both as-synthesized and hot-pressed NiS₂ have a single phase nature, although some hot-pressed
46 samples had traces of the sulfur deficient phase, Ni_{1-x}S (<1%vol), due to the strong
47 desulfurization at T > 340 °C. The electronic band structure and density of states were calculated
48 by Density Functional Theory (DFT), indicating a metallic behavior. However, the electronic
49 transport measurements showed p-type semiconductivity for bulk NiS₂, pointing to the presence
50 of important electron correlation effects that lead to a Mott insulator behavior. The consolidation
51 conditions strongly influence the electronic properties, with the best room-temperature Seebeck
52 coefficient, electrical resistivity and power factor being 182 μVK⁻¹, 2257 μΩm and 14.1 μWK⁻¹
53 m⁻¹, respectively, pointing this compound as a good starting point for a new family of
54 thermoelectric materials.

55

56

57 Introduction

58 The search for new, clean, energy sources, as well as the optimization of their use, has become a
59 major issue in contemporary societies. According to the European Environment Agency, current
60 conventional thermal power plants have an energy efficiency around 35-45%, most of the energy
61 being lost as wasted heat [EEA 2013]. Thermoelectric (TE) materials, which convert thermal
62 energy into electric energy (Seebeck effect) and vice-versa (Peltier effect), are a promising
63 solution to increase the efficiency of many devices and equipment. The potential of a material for
64 thermoelectrics can be evaluated by its figure of merit, $zT = \alpha^2 T / \rho \lambda$, where α , T, ρ and λ are the
65 Seebeck coefficient, absolute temperature, electrical resistivity and thermal conductivity,
66 respectively [Gonçalves & Godart, 2014].

67 Current commercially available TE materials contain rare, expensive and toxic elements, being
68 necessary to develop new, cheap, abundant and environment-friendly alternatives. Metal sulfides
69 are interesting candidates, as they fulfill these requirements [Ge et al., 2016]. Tetrahedrites are
70 cheap and easily available mineral sulfosalts that present large figures of merit and are seen as
71 having good potential for thermoelectric applications [Lu et al., 2016]. Pyrite (FeS₂) is low cost
72 sulfide with simple synthesis and moderate thermoelectric properties [Harada, 1998; Zuñiga-
73 Puelles et al., 2019]. In this compound, the large electrical resistivity and thermal conductivity
74 observed in the pristine material are the major constraints to their practical use. These properties
75 can be tuned to much lower values by changing both the composition and microstructure [Uhlig,
76 2014]. Vaesite (NiS₂), another transition mineral sulfide with pyrite structure [Krill et al., 1976],
77 was reported, but its thermoelectric properties were only poorly explored. At equilibrium

78 conditions, NiS₂ is a stoichiometric compound, stable up to 1020 °C [Waldner & Pelton, 2004].
79 However, previous studies also suggested that vaesite is an intrinsic non-stoichiometric
80 compound, with a variable metal concentration and a stable anion content. These deviations from
81 stoichiometry, corroborated by a change of the cell parameters, have important consequences in
82 the electrical and magnetic properties [Gautier et al., 1972; Krill et al., 1976]. Measurements on
83 single crystals, natural materials and samples prepared by high-pressure synthesis indicated a
84 semiconducting behavior for this compound [Bither et al., 1968; Kautz et al., 1972; Gautier et
85 al., 1972; Krill et al., 1976], which pointed to the possibility of using it as thermoelectric
86 material. Nevertheless, thermoelectric measurements made on thin films showed a p-type
87 semiconducting behavior, but small room temperature Seebeck coefficients, which contrasts with
88 the large values obtained on single crystals prepared by halogen transport [Bither et al., 1968].
89 Moreover, albeit the preparation of synthetic bulk NiS₂ by solid state route has been previously
90 described [Krill et al., 1976; Matsuura et al., 2000], it resulted in highly porous pellets, easily
91 disaggregated, not suitable for the electrical transport properties study. In this work, we explored
92 the solid-state route followed by hot-press to prepare dense vaesite samples, suitable for their
93 characterization, including the electrical transport properties (electrical resistivity and Seebeck
94 coefficient) investigation. Density functional theory calculations were also performed and their
95 results compared with the experimental data.

96

97

98

99

100

101 **Materials & Methods**

102 NiS₂ samples, with an average mass of ~1.5 g, were prepared by high-temperature reacting the
103 elements inside quartz ampoules. The desired quantities of Ni and S were put inside the quartz
104 ampoules (8 mm inner diameter, 1 mm wall thickness), which were evacuated down to
105 6×10^{-5} mbar and sealed. An excess of 5wt% of the chalcogenide element was considered in
106 order to compensate eventual evaporation losses. The ampoules were placed in a horizontal tube
107 furnace pre-heated at 150 °C, and heated at 800 °C for 12 h, with a heating speed of 0.3 °Cmin⁻¹
108 and two intermediate dwells at 400 °C and 650 °C for 8 h. Afterwards, they were slowly cooled
109 inside the furnace. The samples were then manually ground, cold-pressed, sealed in evacuated
110 quartz ampoules and heated again in the same conditions. Finally, the samples were once more
111 manually powdered, a ~30wt% excess of S was added, and ~0.6 g of the resulting powder was
112 charged in a high-density graphite mould that was used in the hot-pressing procedure. The hot-
113 press was made under inert atmosphere (Ar), increasing the pressure at 3 MPa•min⁻¹ up to
114 56 MPa and the temperature at 25 °Cmin⁻¹ up to three different dwell temperatures, 700 °C,
115 720 °C and 750 °C, staying there for 1h30 min. Temperature was then decreased to <100 °C at
116 25 °Cmin⁻¹ and the pressure removed at 3 MPa•min⁻¹.

117 Part of each pellet was manually ground and characterized by powder X-ray diffraction (XRD).
118 A PANalytical X'Pert PRO diffractometer (Bragg-Brentano geometry, Cu K α radiation) was
119 used. The powders were placed in a low-noise Si single crystal XRD holder and 2θ was scanned
120 from 20° to 90° , with a step size of 0.033° and a time per step of 50 s. Phase identification was
121 made through comparison of the collected diffractograms with reference patterns taken from the
122 literature. Cell parameters and theoretical density were calculated and refined from the powder
123 diffraction data, using the Unit-Cell software [Holland & Redfern, 1997]. Experimental values of
124 density were determined by the Archimedes method. Porosity was estimated by image analysis,
125 using the ImageJ software.

126 Optical microscopy, scanning electron microscopy (SEM) and energy-dispersive spectroscopy
127 (EDS) were used for microstructure characterization and chemical composition analysis. It was
128 used an optical microscope ZEISS SteREO Discovery V20 and a JEOL JSM-7001F field
129 emission gun scanning electron microscope (accelerating voltage of 25kV), with an Oxford
130 Instruments EDS spectroscopy system attached.

131 Thermal stability was evaluated with thermogravimetric analysis (TGA). A Dupont 951 Thermo-
132 gravimetric Analyzer was used. Samples were manually grounded, placed in platinum pans, and
133 heated from 25°C to 950°C , at a heating rate of 10°Cmin^{-1} in an inert atmosphere (N_2) flowing
134 at a rate of $60\text{ mL}\cdot\text{min}^{-1}$.

135 The nature of chemical bonding was analysed by Raman spectroscopy, using a Horiba LabRam
136 HR Evolution Raman microspectrometer (laser with $\lambda=532\text{ nm}$ and 10 mW power). Raman
137 spectra were collected from 150 to 1800 cm^{-1} , the laser light being focused with a $100\times$
138 objective. 4 scans, with 30 seconds each, were made for each spectrum. Lower laser powers (25-
139 50% of maximum) were required in some measurements to avoid the surface damage.

140 Electrical transport properties were measured between 20-300 K, at a rate of 0.3 Kmin^{-1} for the
141 Seebeck coefficient and 0.5 Kmin^{-1} for electrical resistivity, using a closed-cycle cryostat. A
142 system based on the Chaikin's device to measure organic single crystals [Chaikin & Kwak,
143 1975] was used to measure the Seebeck coefficient. The samples were first shaped to a plate-like
144 geometry ($\sim 0.5\times 0.5\times 3.5\text{ mm}^3$) and glued with GE varnish to two gold foils (located in two single
145 crystal quartz blocks heated independently), and the foils are glued with GE varnish to the quartz
146 blocks, so that each side of the sample is thermally anchored to one of the blocks. Two gold
147 wires connected to the sample, then establishing the electrical contacts. The voltage was
148 measured with a low frequency AC technique, with a maximum temperature gradient in the
149 sample of 1 K, controlled by two Au-Fe-Chromel thermocouples connected to the quartz blocks.
150 The electrical resistivity was measured in the same bar-shaped samples through the four-point
151 technique, using an AC resistance bridge and a current of 1 mA. Activation energies were
152 obtained from the electrical resistivity data.

153

154 **Band structure calculations**

155 The band structure and density of states of NiS_2 were calculated with the help of the WIEN2k
156 package [Blaha et al., 2018]. Calculations were performed within the density functional theory

157 (DFT), using linear augmented plane wave (LAPW) method to solve the Kohn-Sham equations.
158 Lattice parameters and atomic positions were taken from experimental data [Villars & Calvert,
159 1986]. Both local spin density approximation (LSDA) and generalized gradient approximation
160 with a modified Becke-Johnson potential (GGA+mBJ) were used to approach the exchange-
161 correlation energy [Koller, Trans & Blaha, 2012]. The parametrization developed by Perdew-
162 Burke-Ernzerhof was applied for the generalized gradient approximation (PBE-GGA) [Perdew,
163 Burke & Ernzerhof, 1996]. A cut-off energy of 6 Ry and 1000 k-points in the irreducible part of
164 the Brillouin zone were used for the self-consistent calculations. The criteria of convergence was
165 set at 0.0001 Ry.

166

167

168 Results and discussion

169 The powder X-ray diffraction results always point to single phase samples, both after solid-state
170 reaction and hot-pressing (**Figure 1**). All peaks are indexed to the NiS₂ crystal structure, of cubic
171 Pa3 space group. The lattice parameter after solid-state reaction is $a=5.685(2)$ Å. Lattice
172 constants were also calculated for the pellets densified at different consolidation conditions
173 (**Table 1**), remaining unchanged.

174 The pellets obtained after the initial heating cycle were highly porous and easily disaggregated,
175 in agreement with the previous results [Krill et al., 1976; Matsuura et al., 2000]. Representative
176 microstructures of NiS₂, as-synthesized and hot-pressed, were captured by SEM (**Figure 2**). As-
177 synthesized samples have several pores at the surface, visible to the naked eye, and poorly
178 agglomerated grains. On the other hand, after hot-pressing there is no distinguishable grain
179 boundaries and the porosity decreased substantially (only small closed pores are present)
180 indicating a successful sintering of the grains. The measured compositions, analyzed by EDS, as
181 well as secondary phases detected, are summarized in **Table 2**. The microstructure of all samples
182 is homogeneous, being mainly composed of NiS₂. In samples consolidated at 700 °C/56 MPa and
183 750 °C/56 MPa there is the presence of a sulfur deficient phase, Ni_{1-x}S, but in minor amounts (<
184 1vol%). A small deviation from the nominal composition was observed in all samples.

185 The relative density of the consolidated samples increased with increasing hot-pressing
186 temperature, achieving 97% of the theoretical density when processed at 750 °C and 56 MPa.
187 The high relative densities, >94%, and low estimated porosity, <6% (obtained by image
188 analysis), indicate a successful consolidation of the pellets.

189 Raman spectroscopy was used to characterize the vibrational frequencies specific of the chemical
190 bonds on the hot-pressed samples. Due to their similarity, only one spectrum is shown (**Figure**
191 **3**). The spectra are in qualitative agreement with literature reports [Marini et al., 2011]. Vaesite
192 has five Raman active modes: A_g, E_g and three T_g modes. Since Ni atoms are located at the
193 center of inversion, all Raman active modes correspond to displacements of the sulfur atoms.
194 Two T_g and E_g modes correspond to S-S pairs libration. A_g and a T_g modes correspond,
195 respectively, to in-phase and out-of-phase stretching of the S-S dimers [Marini et al., 2011]. In
196 the collected spectra only four peaks were detected: two peaks at 268 and 278 cm⁻¹,

197 corresponding to $T_g(1)$ and E_g symmetries (S-S libration); a peak at 474 cm^{-1} and a shoulder at
198 485 cm^{-1} , corresponding to A_g and $T_g(2)$ vibrational modes (stretching vibrations). The fifth
199 Raman active mode, $T_g(3)$, is not visible in the spectra and has never been reported before in
200 previous Raman data available in the literature [Marini et al., 2011]. In all the consolidation
201 conditions, the peaks are located at the same shift values and have similar widths, suggesting that
202 the different sintering temperatures do not introduce distortions or strains in the crystal lattice
203 and that the type and number of bonds are similar.

204 The thermal stability of NiS_2 was evaluated by thermogravimetric analysis under N_2 atmosphere,
205 before and after hot-pressing. The results are shown in **Figure 4**. There is a small mass loss at
206 $\sim 80^\circ\text{C}$ for both non-consolidated and consolidated samples, of 4wt% and $<1\text{wt}\%$, respectively,
207 due to dehydration and desorption of chemical species formed during storage under air (the non-
208 consolidated materials was stored for ~ 6 months, while the consolidated was characterized just
209 after the preparation). At higher temperatures, a significant mass drop ($\sim 35\%$) is observed for
210 both samples, due to desulfurization of NiS_2 . The desulfurization starts at $\sim 340^\circ\text{C}$ in the hot-
211 pressed sample and at $\sim 440^\circ\text{C}$ in non-consolidated powders. This difference of almost 100°C is
212 most likely related with the excess of 30% of sulfur added to the samples prior hot-pressing. The
213 real amount of lost sulfur during the hot consolidation was not controlled and therefore, it is
214 possible that not all the sulfur in excess has been evaporated from the pellet, originating a sulfur-
215 saturated vaesite structure. If that happened, then the early sulfur loss can be caused by the
216 excess of sulfur. Previously reported thermogravimetric analysis of elemental sulfur indicate that
217 sulfur starts to evaporate at 200°C and by 320°C the analyzed mass is lost in its total [Takahashi
218 et al., 2015]. If there is excess of sulfur in vaesite structure, then sulfur might start being released
219 at lower temperatures. In order to avoid thermal degradation of NiS_2 and formation of S-deficient
220 phases, the service temperature of these materials should not surpass $\sim 340^\circ\text{C}$. There are no
221 previous studies on the mechanisms of decomposition of vaesite but the similarity with pyrite
222 TGA results [Lambert, Simkovich & Walker, 1998] suggests that NiS_2 might decompose by
223 similar mechanisms of sulfur direct escape from vaesite lattice, followed by a decomposition of
224 NiS_2 into Ni_{1-x}S and subsequently, into NiS .

225 The band structure and density of states of NiS_2 calculated using GGA+mBJ (the LSDA give
226 similar results) are shown in **Figure 5**. From the DFT calculations, one could expect NiS_2 to be
227 metallic due to the partly filled e_g band. The temperature dependence of Seebeck coefficient and
228 electrical resistivity, for the different consolidation conditions, are indicated in **Figures 6 and 7**.
229 Seebeck coefficient, electrical resistivity and power factors at room temperature are shown in
230 **Table 3**. In all samples, the Seebeck coefficient is positive, indicating that the major charge
231 carriers are holes (p-type semiconductor). The incoherence between the theoretical and
232 experimental results can be related to the electron-electron interactions that lead to a Mott
233 insulator, i.e., an insulator material due to strong correlation effects originated by electrostatic
234 repulsion between electrons, which are not accounted for by conventional band theories. The
235 bandgap of vaesite has been reported to be 0.27 eV [Kautz et al., 1972].

236 The highest Seebeck coefficient and power factor were obtained for the pellet hot-pressed at
237 720 °C and 56 MPa. Unlike the other samples, this pellet did not show evidences of secondary
238 sulfur-deficient NiS. No experimental work regarding NiS electrical properties was found, but
239 DFT calculations predict a metallic character [Persson, 2014]. The presence of a metallic phase,
240 even if in small amounts, is expected to be detrimental to the vaesite thermoelectric properties
241 and can be the reason for the lower power factors on the pellets hot-pressed at 700 °C and
242 750 °C. Conversely, the non-presence of NiS in the pellet hot-pressed at 720 °C points to a lower
243 sulfur content on it (that due to the small difference to the 1:2 stoichiometry could not be
244 detected), which is able to affect the Seebeck coefficient. Therefore, a higher Seebeck coefficient
245 does not seem to be related with the aggregation of the samples, but with the sensitivity of the
246 electronic properties (carrier concentration and type, conductivity and mobility) to stoichiometric
247 variations and crystal defects (grain boundaries and impurities).

248 The values of ρ correspond to the values reported in the literature for polycrystalline samples
249 [Gautier et al., 1972; Krill et al., 1976]. A decrease of resistivity is verified with the increase of
250 the hot-pressing temperature. A higher hot-pressing temperature led to a higher aggregation of
251 the grains, translated into a higher relative density and less grain boundary area, resulting in a
252 decrease of the resistivity. The activation energy of these materials is slightly smaller than the
253 one observed in Bi₂Te₃ (**Table 3**) pointing to a possible use as thermoelectric materials close to
254 room temperature. To the best of our knowledge, there are no reported measurements of the
255 Seebeck coefficient of bulk samples. Reported values of α and ρ for single crystals and thin films
256 tend to be higher than the obtained in this work, probably due to the isotropic character of bulk
257 polycrystalline samples. The drop in electrical resistivity curves at 50 K, signaled by an arrow,
258 indicate a magnetic phase transition of NiS₂ from antiferromagnetic to weak ferromagnetic.
259 The electrical resistivity increases with decreasing temperature, indicating a semiconducting
260 behavior. On the other hand, the decrease of the Seebeck coefficient with decreasing temperature
261 contrasts with the resistivity results and could point to multiple bands, with two types of charge
262 carriers.

263

264

265 **Conclusions**

266

267 The preparation of NiS₂ by solid-state route, followed by hot-pressing resulted in single phase
268 pellets. Relative densities superior to 94% were achieved. No significant changes in chemical
269 bonds and lattice distortions were verified for the different hot-pressing conditions.

270 Thermogravimetric analysis of these compounds indicates a strong desulfurization above 340 °C,
271 which limits their service temperature. As opposite to the band structure calculations that
272 suggested a metallic behavior, bulk NiS₂ is a p-type semiconductor. The maximum power factor
273 obtained for vaesite (14.1 $\mu\text{WK}^{-2}\text{m}^{-1}$), which is significantly higher than the pristine pyrite
274 [Zuñiga-Puelles et al., 2019], is a good starting point for further improvements. This work
275 indicates that the consolidation conditions had a notable influence on the resistivity, with denser

276 pellets showing a higher electrical conduction, pointing to an intimate relation between the
277 electronic transport properties and the processing conditions, defects (stoichiometric deviations,
278 grain boundaries) and changes in the chemical composition. Therefore, we can expect that, with
279 a proper optimization of the chemical composition and microstructure, these sulfides could
280 become viable thermoelectric materials.

281 Several aspects were left unexplored in this work. Since the potential of a material for
282 thermoelectricity is also related with its thermal transport properties, a further study of the
283 thermal conductivity is required. The selection of the optimal chemical composition of vaesite,
284 through elemental substitutions, is also necessary. The coupling of these materials in a
285 thermoelectric module also demands good mechanical properties, which so far were never
286 studied. In this project, the thermal stability of vaesite under inert atmosphere was studied but it
287 would be interesting to also evaluate its stability in air (oxidation testing).

288

289

290

291 **References**

- 292 Bither TA, Bouchard RJ, Cloud WH, Donohue PC, Siemons WJ. 1968. Transition metal pyrite
293 dichalcogenides. High-pressure synthesis and correlation of properties. *Inorganic Chemistry*,
294 7(11): 2208–2220. DOI:10.1021/ic50069a008.
- 295 Blaha P, Schwarz K, Madsen GKH, Kvasnicka D, Luitz J, Laskowski R, Tran F, Marks LD.
296 Wien2k - An Augmented Plane Wave+Local Orbitals Program for Calculating Crystal
297 Properties. 2018. Available at:
298 http://susi.theochem.tuwien.ac.at/reg_user/textbooks/usersguide.pdf (accessed at 20 May 2019).
- 299 Chaikin PM, Kwak JF. 1975. Apparatus for thermopower measurements on organic conductors.
300 *Review of Scientific Instruments*, 46(218). DOI: 10.1063/1.1134171.
- 301 Clamagirand JM, Ares JR, Ferrer IJ, Sanchez C. 2012. Near room temperature power factor of
302 metal sulphides films. *AIP Conference Proceedings*, 1449(183). DOI: 10.1063/1.4731527.
- 303 Clamagirand JM, Ares JR, Flores E, Diaz-Chao P, Leardini F, Ferrer IJ, Sanchez C. 2016.
304 Influence of temperature on thermoelectric properties of $\text{Fe}_x\text{Co}_{1-x}\text{S}_2$ thin films: A semiconductor
305 to semimetal conversion. *Thin Solid Films*, 600:19–24. DOI: 10.1063/1.4731527.
- 306 European Environment Agency. Overview of the European energy system. 2013. Available at
307 [https://www.eea.europa.eu/data-and-maps/indicators/overview-of-the-european-energy-system-](https://www.eea.europa.eu/data-and-maps/indicators/overview-of-the-european-energy-system-3/assessment)
308 [3/assessment](https://www.eea.europa.eu/data-and-maps/indicators/overview-of-the-european-energy-system-3/assessment) (accessed at 20 May 2019).
- 309 Ferrer IJ, Sanchez C. 1999. Synthesis of NiS_2 thin films - Electrical and optical properties.
310 *Journal of Materials Processing Technology*, 92-93:239–242. DOI: 10.1016/S0924-
311 0136(99)00172-7.
- 312 Gautier F, Krill G, Lapierre MF, Robert C. 1972. Influence of Non-Stoichiometry on the
313 Electrical and Magnetic Properties of NiS_2 . *Solid State Communications*, 11:1201-1203. DOI:
314 10.1016/0038-1098(72)90824-1.

- 315 Ge ZH, Zhao L, Wu D, Liu X, Zhang B, Li J, He J. 2016. Low cost, abundant binary sulfides as
316 promising thermoelectric materials. *Materials Today*, 19(4):227-239. DOI:
317 10.1016/j.mattod.2015.10.004.
- 318 Gonçalves AP, Godart C. 2014. New promising bulk thermoelectrics: intermetallics, pnictides
319 and chalcogenides. *The European Physical Journal B*, 87(42). DOI: 10.1140/epjb/e2014-40989-
320 3.
- 321 Harada T. 1998. Transport properties of iron dichalcogenides FeX_2 ($X = \text{S, Se and Te}$). *Journal*
322 *of the Physical Society of Japan*, 67(4): 1352-1358. DOI: 10.1143/JPSJ.67.1352.
- 323 Holland TJB, Redfern SAT. 1997. Unit cell refinement from powder diffraction data: the use of
324 regression diagnostics. *Mineralogical Magazine*, 61(404):65-77. DOI:
325 10.1180/minmag.1997.061.404.07.
- 326 Kautz RL, Dresselhaus MS, Adler D, Linz A. 1972. Electrical and Optical Properties of NiS_2 .
327 *Physical Review B*, 6(6):2078-2082. DOI: 10.1103/PhysRevB.6.2078.
- 328 Koller D, Tran F, Blaha P. 2012. Improving the modified Becke-Johnson exchange potential.
329 *Physical Review B*, 85:155109. DOI: 10.1103/PhysRevB.85.155109.
- 330 Krill G, Lapierre MF, Gautier F, Robert C, Czjzek G, Fink J, Schmidt H. 1976. Electronic and
331 magnetic properties of the pyrite-structure compound NiS_2 : Influence of vacancies and copper
332 impurities. *Journal of Physics C: Solid State Physics*, 9:761-782. DOI: 10.1088/0022-
333 3719/9/5/016.
- 334 Lambert JM, Simkovich G, and Walker J.PL. 1998. The Kinetics and Mechanism of the Pyrite-
335 to-Pyrrhotite Transformation". *Metallurgical and Materials Transactions B*, 29B(2):385–396,
336 1998. DOI: 10.1007/s11663-998-0115-x.
- 337 Lu X, Morelli DT, Tetrahedrites: Earth-Abundant Thermoelectric Materials with Intrinsically
338 Low Thermal Conductivity, In *Materials Aspect of Thermoelectricity*, editor Ctirad Uher (Taylor
339 & Francis Group, Boca Raton, CRC Press, 2016).
- 340 Marini C, Perucchi A, Chermisi D, Dore P, Valentini M, Topwal D, Sarma DD, Lupi S,
341 Postorino P. 2011. Combined Raman and Infrared investigation of the insulator-to-metal
342 transition in $\text{NiS}_{2-x}\text{Se}_x$ compounds. *Physical Review B*, 84(23):235134. DOI:
343 10.1103/PhysRevB.84.235134.
- 344 Matsuura M, Hiraka H, Yamada K, Endoh Y. 2000. Magnetic Phase diagram and Metal Insulator
345 Transition of $\text{NiS}_{2-x}\text{Se}_x$. *Journal of Physical Society of Japan*, 69(5):1503-1508. DOI:
346 10.1143/JPSJ.69.1503.
- 347 Perdew JP, Burke K, Ernzerhof M. 1996. Generalized Gradient Approximation Made Simple.
348 *Physical Review Letter*, 77(18):3865-3868. DOI: 10.1103/PhysRevLett.77.3865.
- 349 Persson K. 2014. Materials Data on NiS by Materials Project. Available at
350 <https://materialsproject.org/materials/mp-1547/> (accessed at 2019-06-13).
- 351 Takahashi T, Yamagata M, Ishikawa M. 2015. A sulfur–microporous carbon composite positive
352 electrode for lithium/sulfur and silicon/sulfur rechargeable batteries. *Progress in Natural*
353 *Science: Materials International*, 25(6):672–681. DOI: 10.1016/j.pnsc.2015.11.011

- 354 Uhlig C, Guenes E, Schulze AS, Elm MT, Klar PJ, Schlecht S. 2014. Nanoscale FeS₂ (Pyrite) as
355 a Sustainable Thermoelectric Material. *Journal of Electronic Materials* 43: 2362-2370. DOI:
356 10.1007/s11664-014-3065-x
- 357 Villars P, Calvert LD. 1986. *Pearson's Handbook of Crystallographic Data for Intermetallic*
358 *Phases*. American Society for Metals.
- 359 Waldner P, Pelton AD. 2004. Thermodynamic Modeling of the Ni-S System. *Zeitschrift für*
360 *Metallkunde*, 95(8):672-681. DOI: 10.3139/146.018005.
- 361 Zuñiga-Puelles E, Cardoso-Gil R, Bobnar M, Veremchuk I, Himcinschi C, Hennig C, Kortus J,
362 Heide G, Gumeniuk R. 2019. Thermoelectric performance of high quality bulk synthetic and
363 natural pyrites (FeS₂). *Dalton Transactions*, accepted manuscript.

Table 1 (on next page)

Comparison of physical properties of NiS₂, at different consolidation conditions.

1
2

Consolidation conditions	Porosity (%)	Lattice constant (Å)	Theoretical density (g/cm ³)	Apparent density (g/cm ³)	Relative density (%)
HP at 700°C/56MPa	6±1	5.687(6)	4.435	4.18±0.01	94
HP at 720°C/56MPa	6±1	5.686(4)	4.437	4.20±0.07	95
HP at 750°C/56MPa	4±1	5.687(8)	4.434	4.31±0.02	97

3
4

Table 2 (on next page)

Measured composition and secondary phases detected by EDS.

1

Consolidation conditions	Measured composition	Secondary phases
HP at 700°C/56MPa	$\text{NiS}_{2\pm 0.06}$	Ni_{1-x}S ($x=0.11$)
HP at 720°C/56MPa	$\text{NiS}_{2.05\pm 0.02}$	Not detected
HP at 750°C/56MPa	$\text{NiS}_{2\pm 0.05}$	Ni_{1-x}S ($x=0.12$)

2

3

Table 3 (on next page)

Activation energy (E_a), room temperature Seebeck coefficient (α), electrical resistivity (ρ) and power factor (PF) of NiS₂ hot-pressed at different temperatures.

1
2

Consolidation conditions	E_a (meV)	α_{300K} ($\mu\text{V/K}$)	ρ_{300K} ($\mu\Omega\text{m}$)	PF_{300K} ($\mu\text{WK}^{-2}\text{m}^{-1}$)
HP at 700°C/56MPa	43	128	3230	5.1
HP at 720°C/56MPa	64	182	2350	14.1
HP at 750°C/56MPa	68	119	2257	6.3

Figure 1

XRD diffractograms of as-synthesized NiS_2 and hot-pressed at different temperature conditions. Reference pattern of NiS_2 in gray [Villars & Calvert, 1986].

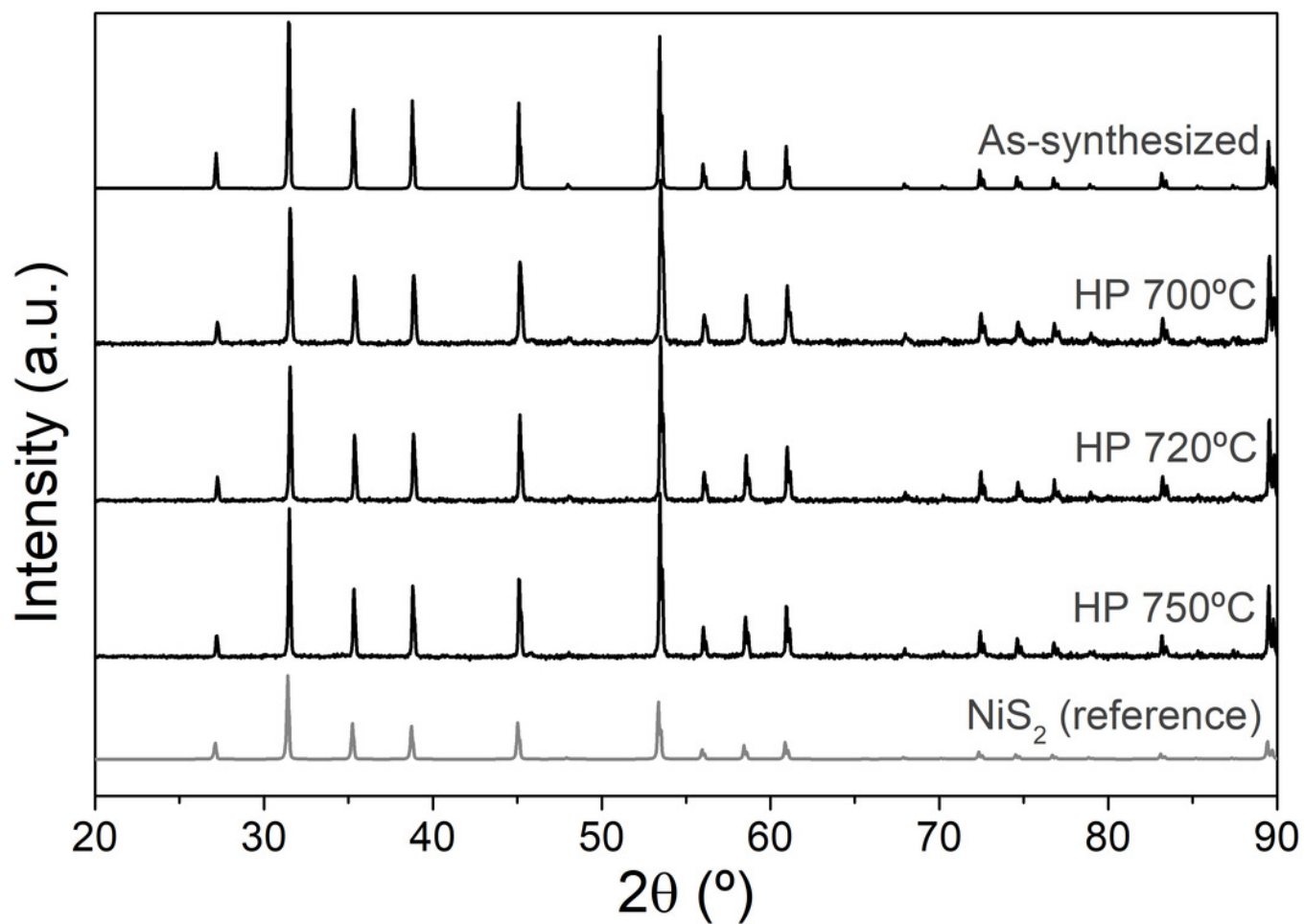


Figure 2

Optical and SEM images of as-synthesized NiS_2 ,

captured by (a) optical microscope (20x) and (b) SE-SEM (1000x magnification). BS-SEM

(500x) images of NiS_2 hot-pressed at 56MPa for 1,5h, at different temperatures: (c)700°C, (b)

720°C, (c) 750°C. P - Pores, B - Sulfur-deficient phase Ni_{1-x}S .

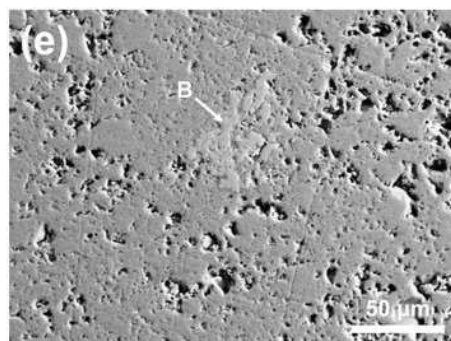
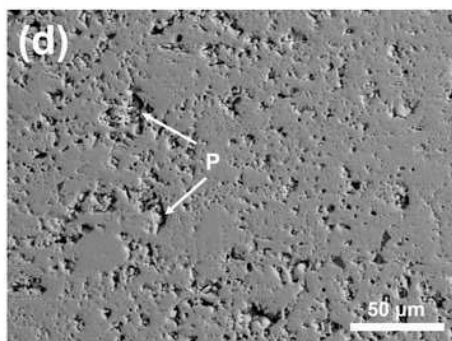
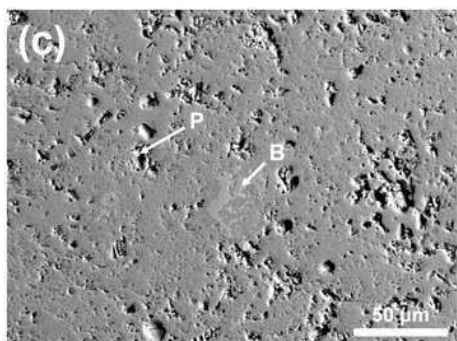
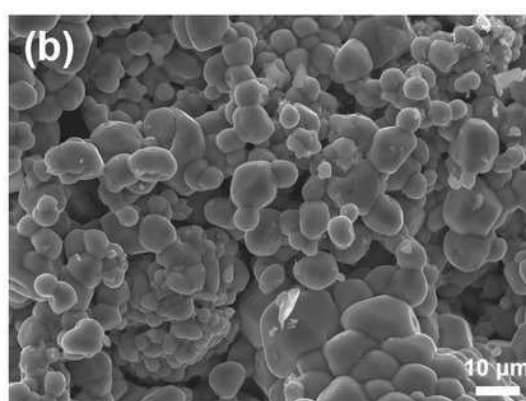
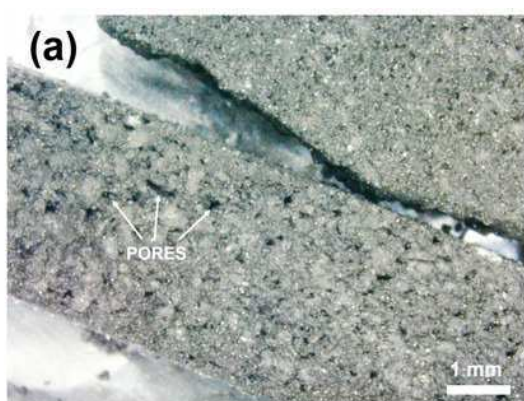


Figure 3

Raman spectrum of hot-pressed NiS₂.

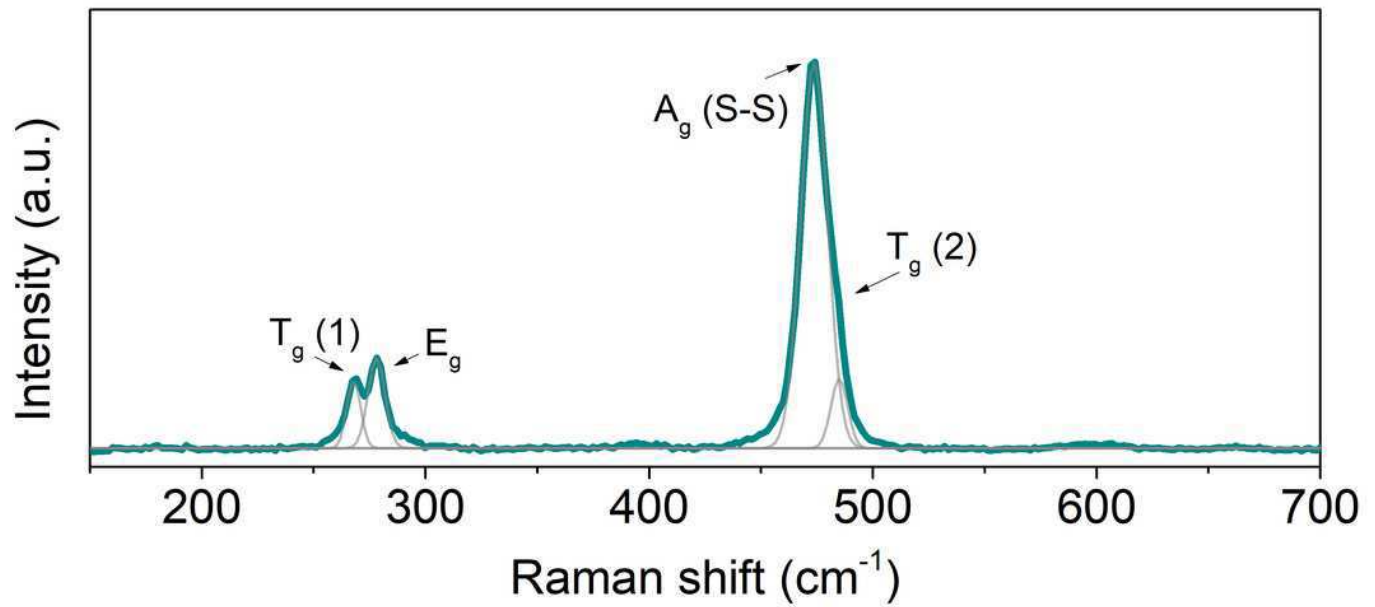


Figure 4

Thermogravimetric analysis of as-synthesized and hot-pressed NiS_2 .

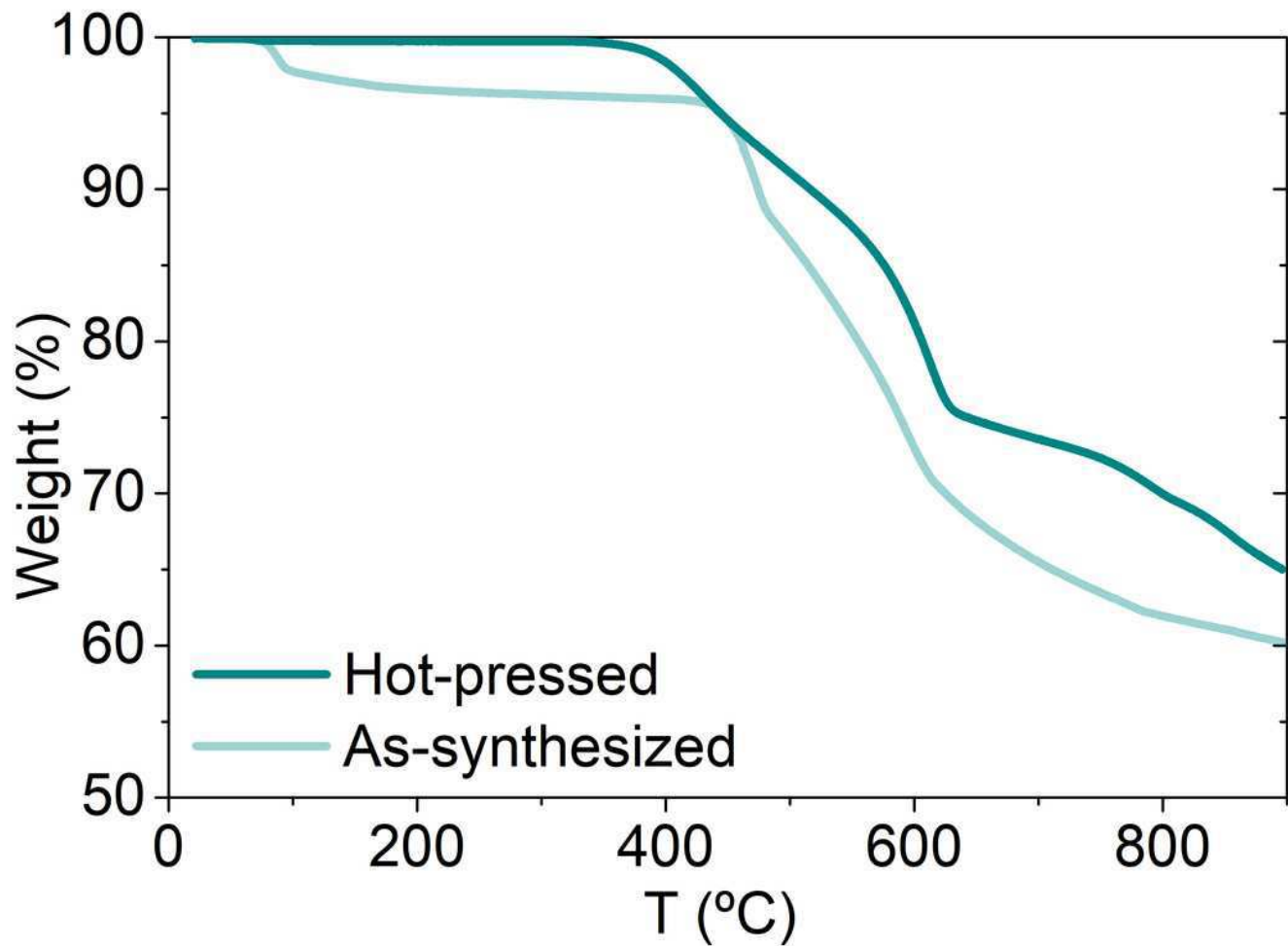


Figure 5

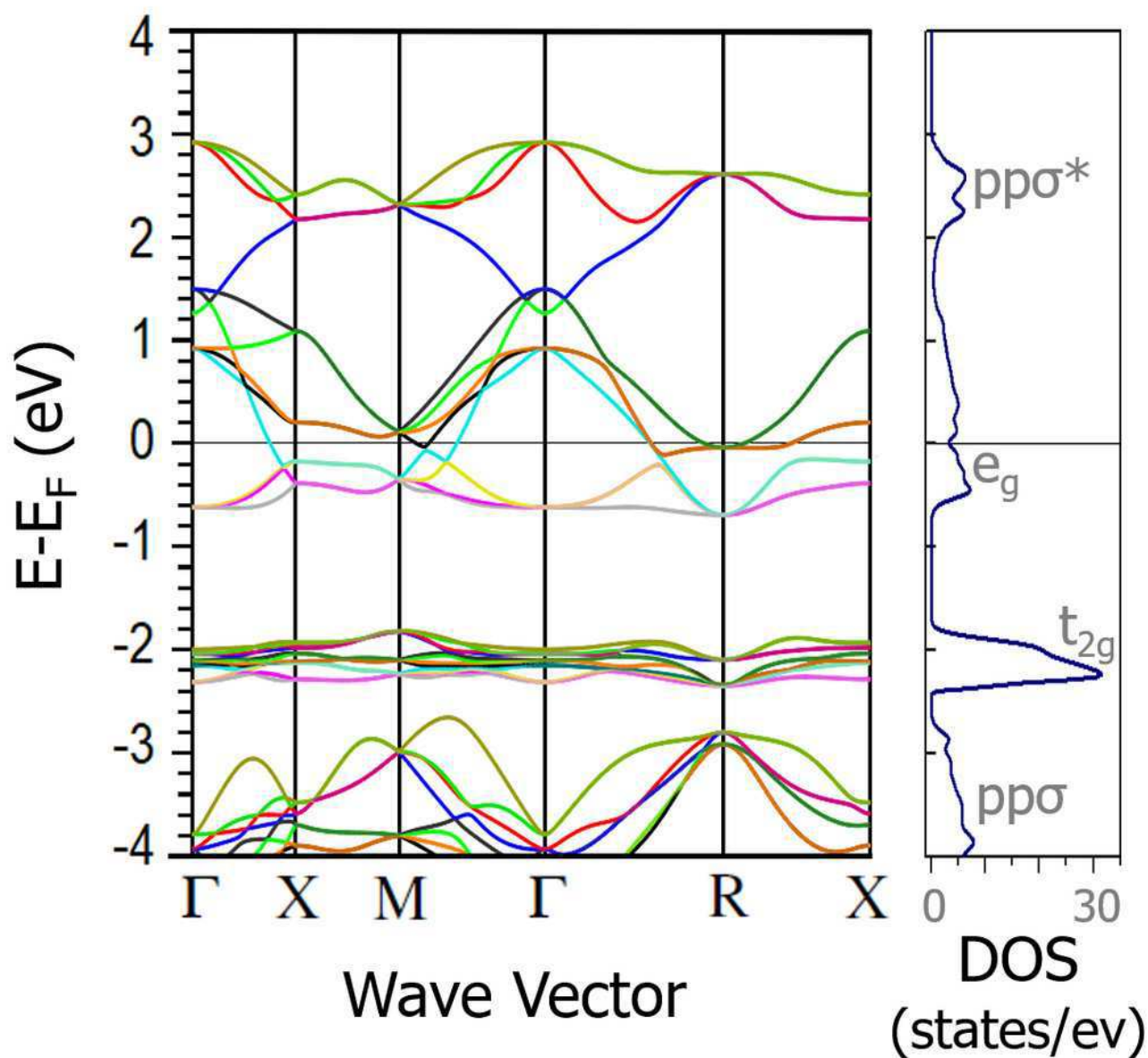
Band structure and density of states DFT calculations of NiS₂.

Figure 6

Temperature dependence of Seebeck coefficient of NiS_2 , at different consolidation conditions.

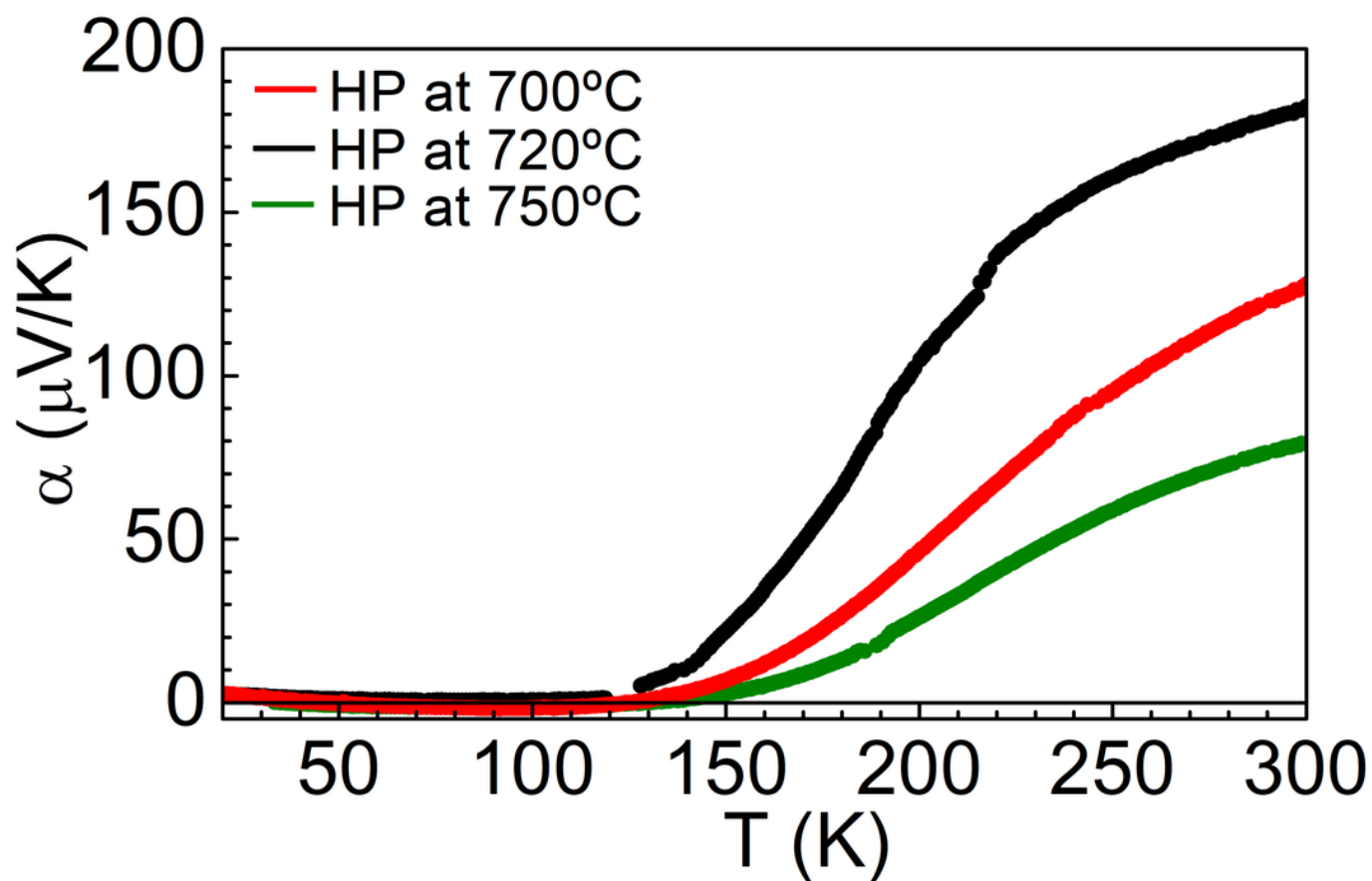


Figure 7

Temperature dependence of electrical resistivity of NiS_2 , at different consolidation conditions.

